Journal of Materials Chemistry B

RSC Publishing

PAPER

View Article Online
View Journal

Cite this: DOI: 10.1039/c3tb21145b

Engineered clathrin nanoreactors provide tunable control over gold nanoparticle synthesis and clustering

Alia P. Schoen,[ab] Kelly N. L. Huggins[ab] and Sarah C. Heilshorn*[ab]

The use of biomolecules to direct nanomaterial synthesis has been an area of growing interest due to the complexity of structures that can be achieved in naturally occurring systems. We previously reported the functionalization of self-assembled clathrin protein cages to enable synthesis of nanoparticles from a range of inorganic materials. Here, we investigate the ability of this engineered biomolecule complex to act as a tunable nanoreactor for the formation of different arrangements of gold nanoparticles in three dimensions. We find that self-assembled clathrin cages functionalized with engineered bi-functional peptides induce formation of gold nanoparticles to generate solutions of either dispersed or clustered gold nanoparticles on demand. The 3D arrangement of nanoparticles is dependent on the concentration of the engineered peptide, which fulfills multiple roles in the synthesis process including stabilization of the nanoparticle surface and localization of the nanoparticles within the self-assembled clathrin cage. We propose and evaluate a mechanism that allows us to predict the peptide concentration at which the nanoreactor behavior switches. This work provides insight into peptide-based surfactants and the potential for incorporating them into strategies for tuning biological mineralization processes in mild solution conditions to generate complex structures.

Received 14th August 2013
Accepted 25th October 2013

DOI: 10.1039/c3tb21145b

www.rsc.org/MaterialsB

Introduction

Surfactant molecules are a ubiquitous feature of all solution-based nanomaterial synthesis. They provide stabilization of the grown nanoparticles to prevent agglomeration as well as interact with individual crystalline facets of the synthesized particles to provide size and shape control. Traditional synthesis strategies use organic molecules as surfactants to achieve control over nanomaterial growth. Some common examples are citrate,[1,2] poly(vinyl pyrrolidone),[3] and cetyltrimethylammonium bromide (CTAB)[4,5] which lead to formation of nanoscale particles and wires in various solution conditions. As an alternative to these traditional organic chemistry approaches, biomolecules provide an expanded library of structures and chemical functionalities. There is a growing interest in the use of DNA,[6,7] viruses,[8–10] and proteins[11–14] as surfactants and agents to direct nanomaterial synthesis due to the mild solution conditions required and the potential for mimicking biological mineralization processes that lead to complex ordered structures.

Proteins in particular offer a versatile platform for manipulating chemistry and materials at the nanoscale. Many protein-based approaches use a single component to act as both a site for heterogeneous nucleation and as a surfactant to stabilize the inorganic nanoparticles. For example ferritin, a small cage-like protein assembly, has been used to generate nanoparticles of a range of materials including cadmium sulfide,[15] gold,[16] and iron oxide.[17] Additional functionalities and specificity have been added to protein scaffolds through chemical or genetic modifications enabling formation of a wide range of inorganic materials including zinc oxide nanowires[18] and palladium nanoparticles.[19] Taken together, these systems illustrate the potential of proteins as effective synthesis-directing molecules for a wide range of inorganic nanomaterials. However, tunability of individual reactions is generally limited to forming a single morphology, for example nanowires or dispersed nanoparticles, or a single material. Each different desired synthesis product often requires a newly engineered protein. To address these limitations, we have designed a multi-component system to direct both the synthesis and 3D arrangement of inorganic nanoscale materials.

One advantage of using proteins is their ability to interact through site-specific molecular recognition events. Previously we demonstrated effective use of multiple protein components interacting through engineered molecular recognition to generate a range of inorganic nanoparticle species from a single native protein scaffold.[20] This strategy, termed template engineering through epitope recognition (TEThER) combined a clathrin scaffold protein with engineered peptides to achieve site-specific nanoparticle nucleation and growth. Clathrin is a protein made of three semi-flexible legs, each about 50 nm long,

[a]Materials Science & Engineering, Stanford University, Stanford, CA 94305, USA. E-mail: heilshorn@stanford.edu

[b]Stanford Institute for Materials and Energy Science, SLAC National Accelerator Laboratory, Menlo Park, CA 94025, USA

that form a triskelion structure with three-fold symmetry that self-assembles *in vitro* to form cage structures 50–100 nm in diameter.[21,22] Our functionalized clathrin structures were used to synthesize single nanoparticle suspensions of titanium dioxide, cobalt oxide, and gold.[20] In this study we extend this work to tunable synthesis and organization of gold nanoparticles in 3D space using this complex of separate biomolecules both to provide structure as a surfactant as well as to actively interact and localize nanoparticles during and after synthesis. This work provides mechanistic insight into the multifaceted roles of the different components in our engineered system that may be extended to other protein surfactant systems.

Gold nanoparticles have been used in a variety of biomedical applications and show interesting catalytic properties at the nanoscale.[23] Nanoscale gold both in single particle form as well as in clusters has interesting and highly tunable optical properties potentially useful for a variety of applications, particularly in sensing and imaging.[24–26] Here we show that two separate synthesis regimes can be accessed leading to dispersed or clustered solutions of gold nanoparticles using the same combination of engineered peptide and self-assembled clathrin scaffold. By changing the concentration, and hence function, of the bi-functional peptide component, this surfactant complex becomes a tunable nanoreactor for synthesis of either dispersed nanoparticles or nanoparticle clusters in mild solution conditions.

Results & discussion

Gold nanoparticles were synthesized using a complex of clathrin cages and engineered TEThER peptides based on previously reported protocols. The sequence of the 25 amino acid TEThER peptide (TP-Au) used in this work is KDVSLLDLDDFNGGGGAHHAHHAAD.[20] The clathrin binding sequence (KDVSLLDLDDFN) has been shown to bind to a specific epitope on the clathrin N-terminus which is displayed on the inside of an assembled clathrin cage structure called the "clathrin box" (Fig. 1).[21,27,28] The gold binding sequence (AHHAHHAAD) is a histidine-rich epitope from the HRP II protein in *Plasmodium falciparum* chosen based on previous evidence that it can mediate formation of gold nanoparticles.[29,30] Fixed self-assembled clathrin cages in potassium phosphate buffer, pH 7.0, were mixed with TP-Au or an equal volume of water. Chloroauric acid ($HAuCl_4$) was introduced, and all samples were incubated overnight in the dark to prevent photoreduction.

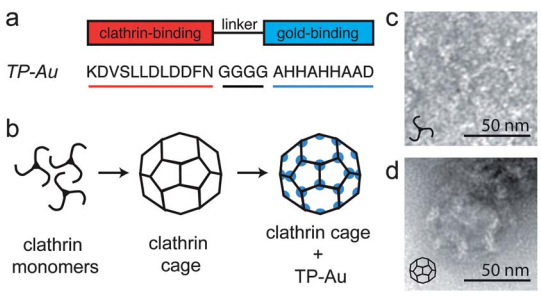

Fig. 1 (a) Schematic and amino acid sequence of the TP-Au peptide. (b) Schematic representation of clathrin self-assembly and functionalization. Blue circles represent TP-Au peptide bound to specific sites on the inside of the assembled clathrin cage. (c and d) Representative transmission electron micrographs (TEM) of clathrin monomers (c) and self-assembled cages (d) stained with uranyl acetate. Schematics are shown in bottom left corner of each image.

Depending on the concentration of TEThER peptide present, the clathrin acts as a nanoreactor to generate dispersed solutions or clusters of gold nanoparticles. This suggests the TP-Au plays different roles in the various reaction conditions. In control reactions with clathrin alone the sample contained purple precipitate at the bottom of the tube of clear liquid (Fig. 2a). TEM analysis showed large gold aggregates indicating uncontrolled growth when no TP-Au peptide is present in solution (Fig. 2b). Similar to previous reports, control samples with only TP-Au peptide (135 μM) and no clathrin cages did not result in gold growth of any kind.[20] In contrast, TP-Au concentration-dependent color differences were observed between samples containing both clathrin cages and TP-Au peptide which all remained as colloidal suspensions (Fig. 2a). TEM analysis of these samples revealed gold nanoparticles in all cases (Fig. 2b).

Samples at the highest TP-Au concentrations tested in combination with clathrin cages, 135 and 67.5 μM, contain clusters of distinct gold nanoparticles and exhibit a purple to purple-red color. At TP-Au concentrations of 33.8 μM and below, the particles are not clustered but instead dispersed in solution, which is bright red in color. Irregular aggregates of fused gold particles are seen in the templating reaction with a TP-Au concentration of 4.3 μM, and the solution is purple. It has been suggested that the histidine-rich peptide sequence used in TP-Au acts as a surface capping agent to stabilize gold nuclei and passivate the surface, and the gold particle grows by adding reduced gold atoms to the surface.[29] We reason that at low peptide concentrations, the surfaces are not sufficiently passivated and particles fuse as they encounter each other in solution to lower their surface energy. This is consistent with the micrographs of the reaction using 4.3 μM TP-Au sample, which show large aggregates of smaller particles. These data suggest that the primary function of the TP-Au peptide in gold nanoparticle synthesis reactions is surface stabilization, while at high enough concentration, the peptide is also able to mediate particle clustering.

Absorbance data support the microscopy data showing that the action of the clathrin nanoreactor can be fine-tuned by modulating TEThER peptide concentration and hence function. A typical plasmon resonance maximum for dispersed gold nanoparticles occurs between 500 and 550 nm with the specific wavelength and peak shape determined by the details of particle size and shape.[31] In addition, particles of identical size and shape can exhibit different resonance behavior depending on clustering.[31,32] UV-vis spectroscopy of the reaction solutions show that while a solution may be 'red' or 'purple,' each reaction condition has its own unique spectral signature indicating subtle differences in the particle morphology (Fig. 3a). The resonance maxima of all solutions fall between 515 and 540 nm

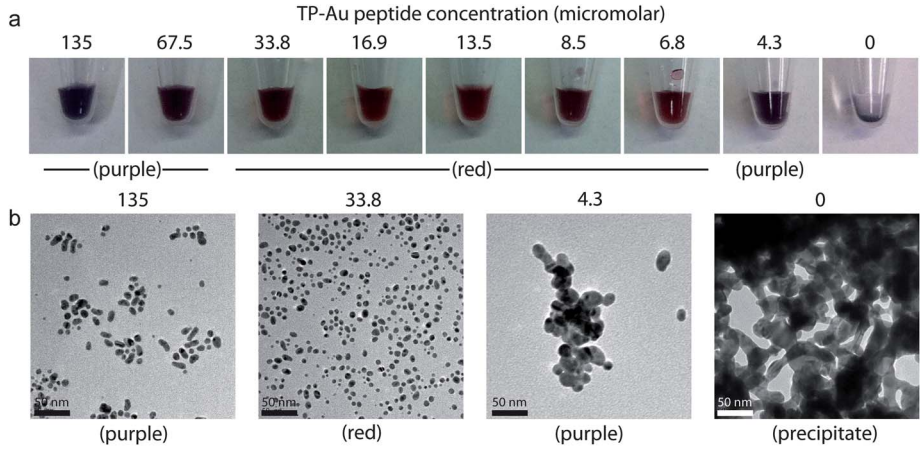

Fig. 2 (a) Photographs of gold nanoparticle synthesis reactions containing clathrin cages and TP-Au at the indicated concentrations after overnight incubation. (b) TEM micrographs of synthesis products from reactions at indicated TP-Au concentrations after overnight incubation.

and shift depending on the peptide concentration (Fig. 3b). In addition, the shape of the plasmon resonance peak changes with peptide concentration, with the highest and lowest concentrations both showing a significant red-shifted shoulder. An increase in size, anisotropy, and clustering of gold nanoparticles are all known to cause red shifts. In our solutions these red shifts are associated with solutions of individual particles that are clustered together but separate (highest TP-Au

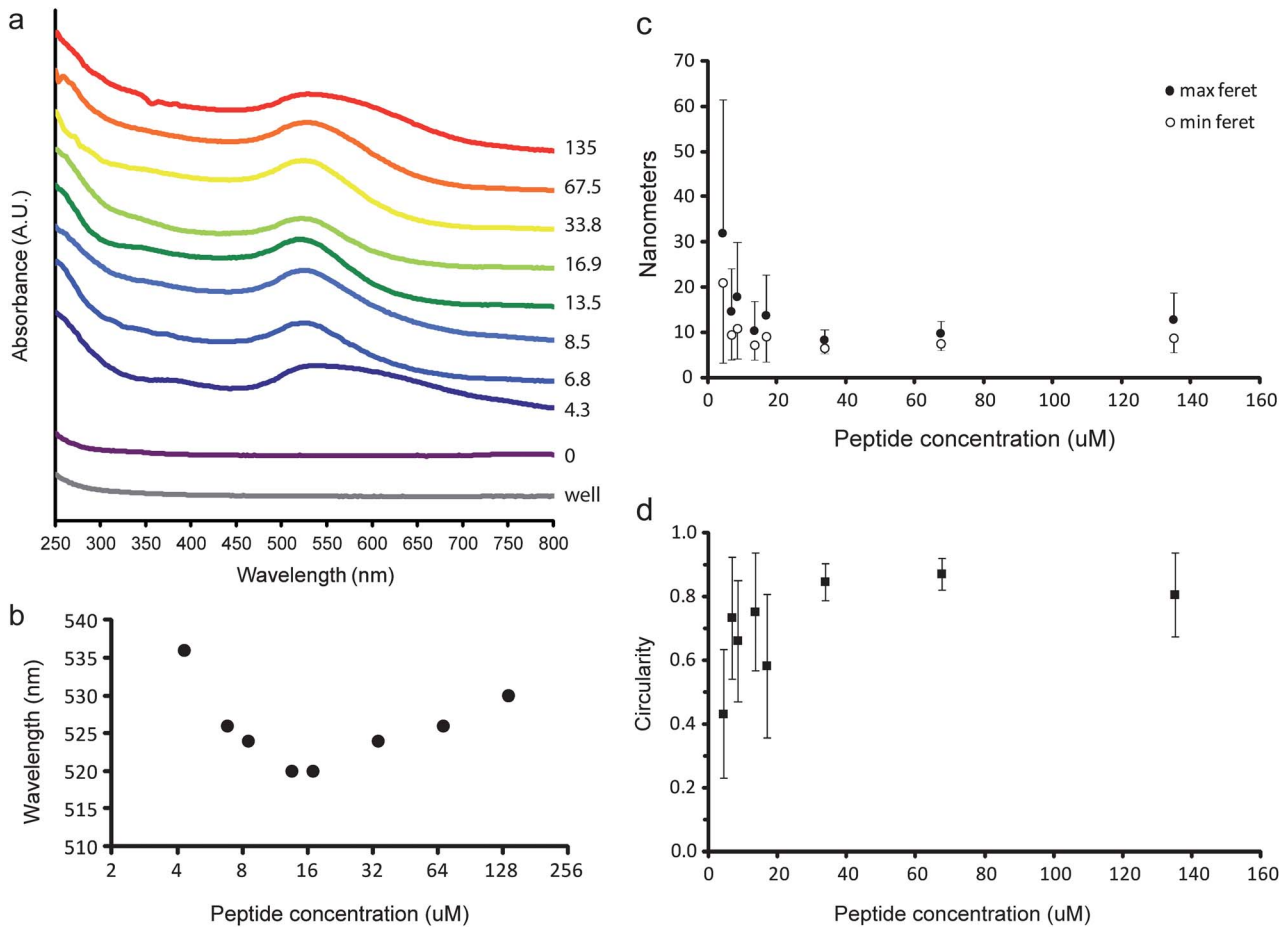

Fig. 3 (a) UV-vis spectra of reaction solutions shown on an offset scale for comparison. TP-Au concentration of each reaction is shown to the right of the curve. (b) Wavelength at the maximum of the surface plasmon peak from the data in (a). (c) Particle diameter (Feret diameter) as a function of peptide concentration as measured from TEM images. Error bars are standard deviation. (d) Particle circularity as a function of peptide concentration as measured from TEM images. Error bars are standard deviation.

concentrations) or with a solution of fused aggregates (lowest TP-Au concentrations) (Fig. 3b). We hypothesize that the purple color at the highest peptide concentrations primarily indicates the proximity of the gold particles to each other while at the lower concentrations the resonance peak is primarily reflective of the size and shape of the gold nanoparticles.

To evaluate this conjecture, TEM was utilized to quantify nanoparticle size, shape, and clustering. Overall the sizes, whether in discrete clusters or dispersed, fall within a range of 10–20 nm (Fig. 3c). The particles are near circular for synthesis reactions with peptide concentrations above ~30 μM, but more irregular as peptide concentration decreases, which is consistent with nanoparticle aggregation (Fig. 3d). Interestingly, at the two highest peptide concentrations clusters formed from distinct nanoparticles are observed, but the particles in the reaction with 67.5 μM TP-Au exhibit higher circularity than those in the reaction with 135 μM TP-Au. Study of a different gold-binding peptide motif suggests that the peptides inhibit surface reactions, *i.e.* the addition of gold atoms to the surface.[33] If an excess of peptide is present in the reaction it is possible that the surface is strongly passivated and growth occurs in directions where the peptides may not be coordinated to the surface as efficiently. This phenomenon would result in an irregularly shaped particle such as those in the reaction using 135 μM TP-Au. In contrast, in a case where there is less peptide in solution, the surface will not be as strongly passivated, and the particle will grow isotropically producing a spherical structure as found in the reaction using 33.8 μM TP-Au.

To examine the kinetics of the clathrin nanoreactor, templating reactions were monitored during the first two hours after initiation. Photographs of the reaction solutions over time show that each reaction turns purple within the first 15 minutes regardless of TP-Au concentration, but that over time reactions with lower concentrations of peptide change color to reddish-purple or red in a TP-Au concentration-dependent manner (Fig. 4). This result suggests that each reaction begins in a similar fashion but is then modified during particle growth depending on the concentration of TP-Au, which may have a similar role in all reactions at early times and then change function as the reactions progress.

To assess whether these reactions are in fact following a similar growth pathway in the early stages of nucleation and growth or if the mechanism of early-stage growth is different, reactions were run at two peptide concentrations that result in different final colors, 135 μM and 33.8 μM. Both reaction solutions appear purple after 15 minutes, however overnight the sample with 135 μM TP-Au remains purple while the reaction with 33.8 μM TP-Au turns red. TEM analysis of the overnight samples shows that the gold nanoparticles are clustered in the reaction containing clathrin cages and 135 μM TP-Au, while the particles are dispersed in the reaction containing clathrin cages and 33.8 μM TP-Au (Fig. 5). In contrast, TEM micrographs of the 15 minute time point show that the gold nanoparticles, which are similar in size, are clustered in both cases indicating that the nucleation and early-stage growth of gold nanoparticles is the same at the two peptide concentrations. This suggests that the TP-Au peptide controls stabilization of the particle surfaces in the same way in both reactions but mediates clustering of the gold particles differently at earlier and later time points.

The TP-Au peptide is designed to bind to a specific site on the inside of an assembled clathrin cage. Our previous work has

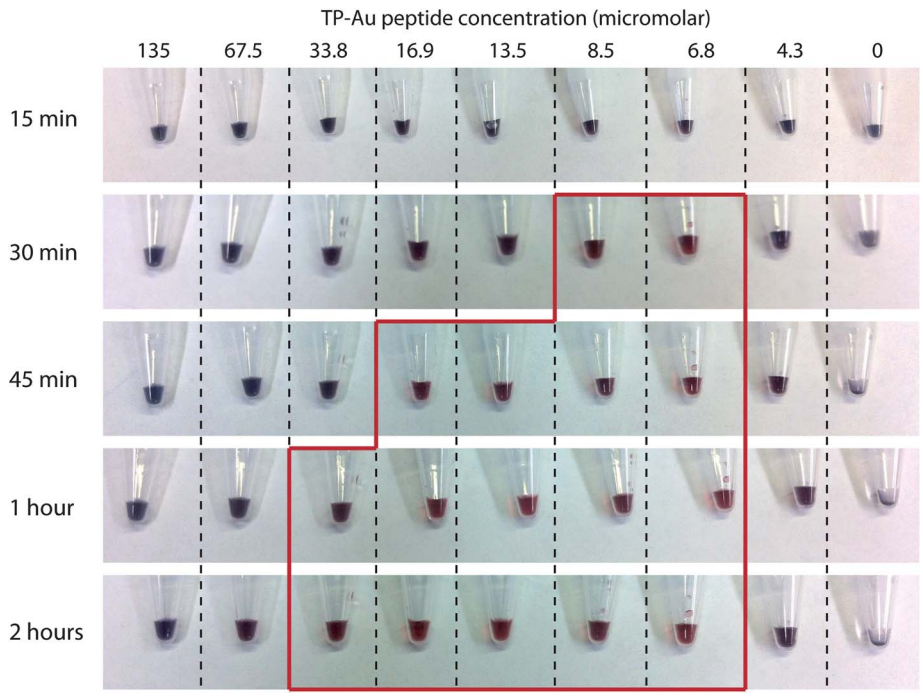

Fig. 4 Photographs of gold nanoparticle synthesis reactions containing clathrin cages and indicated concentrations of TP-Au. Reactions were monitored and photographed at the times shown to the left. Tubes inside the red box all contain red solutions, outside the box the solutions are purple.

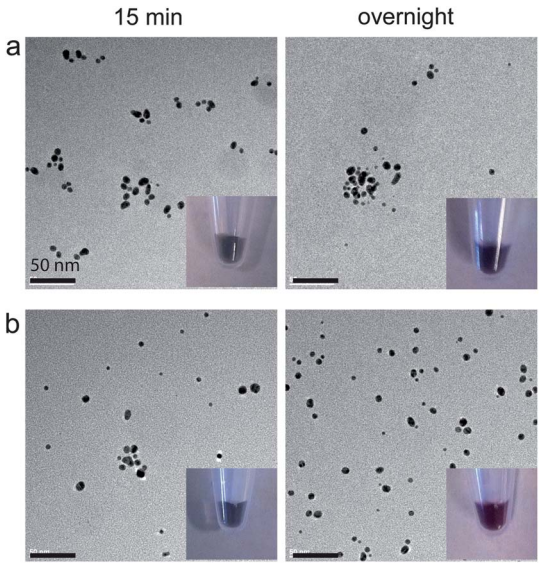

Fig. 5 TEM micrographs of gold nanoparticle synthesis reactions containing clathrin cages and 135 μM (a) or 33.8 μM TP-Au (b) at 15 minutes and overnight time points. Insets: photographs of the synthesis reactions at the corresponding time point.

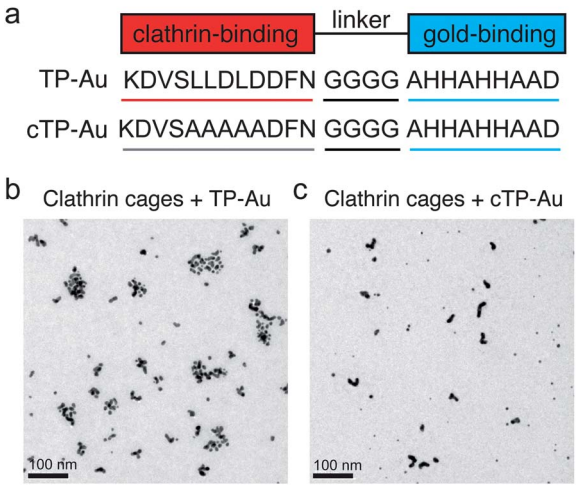

Fig. 6 (a) Peptide schematic and amino acid sequences of TP-Au which binds a specific site inside clathrin cages and control peptide cTP-Au which cannot bind clathrin. (b and c) TEM micrographs of gold nanoparticle synthesis reactions containing clathrin cages and 135 μM TP-Au (b) or cTP-Au (c).

shown that at early time points in the gold templating reaction, multiple gold nuclei are present inside the clathrin cage.[20] In the reactions shown here the clustering is apparently preserved in some cases as the particles grow and is still observed in solution after hours of incubation. To confirm that the clustering present after overnight incubation is the result of this specific scaffold-peptide binding, a control TEThER peptide was generated that replaced important amino acids that mediate binding to the clathrin scaffold with alanine. This change eliminates the functional side chains of the substituted amino acids but keeps the overall peptide backbone length the same. The control TEThER peptide (cTP-Au) sequence is KDVS*AAAAA*DFNGGGGAHHAHHAAD (modified amino acids are shown in italics). In reactions with 135 μM of cTP-Au, no clustering was observed compared to an identical reaction using the unmodified TP-Au where robust clustering of distinct nanoparticles was seen (Fig. 6). Therefore the peptides tethered to the inside of the cage are responsible for the clustering of the gold particles, which in turn suggests the clusters are groups of particles still inside the clathrin cage scaffolds after long reaction times. This data confirms the second role of the TP-Au peptide in gold nanoparticle synthesis, localization of particles within the clathrin cages.

Knowing that clathrin cages alone will reduce gold to generate aggregates and that peptide alone does not produce nanoparticles for our reaction conditions, we reason that the peptides are in fact primarily acting as surfactants to stabilize the surface of the particles rather than directly inducing gold reduction consistent with observations by Slocik *et al.*[29] Additionally, once peptide is coordinated on the particle surface, the clathrin-binding domain of the peptide acts to bind the growing particle to the clathrin scaffold at a specific site inside the clathrin cage. In the samples using cTP-Au and concentrations of intact TP-Au from 33.8–6.8 μM, dispersed particles are observed indicating that particles can be released outside of the clathrin cages. These dispersed particle solutions imply that particles nucleated inside the clathrin scaffold must leave the cage to continue growth before they get too large to travel out of the openings in the cage faces (which are ~10–20 nm in diameter). It is straightforward to understand how this occurs in the cTP-Au case: gold ions are reduced to form nuclei which are stabilized by the gold-binding motif in the cTP-Au peptide and are free to diffuse around the clathrin cages in solution since the peptide has no clathrin-binding ability. In contrast, for the TP-Au peptide, which does have clathrin-binding ability, our data demonstrate that the role of the peptide is controlled by its concentration in the reaction mixture.

One proposed mechanism is that as a particle grows, peptides bind to the surface non-specifically through the clathrin-binding sequence as well as binding the surface specifically through the histidine-rich epitope. Below a certain peptide concentration, this would result in a particle completely coated with peptide but without any available clathrin-binding domains leading to a scenario similar to the cTP-Au reaction (Fig. 7a bottom). The particles would have no specific clathrin-binding epitope available on their surfaces and would therefore be dispersed in solution. At higher concentrations of peptide, the more favorable gold–histidine interaction would outcompete non-specific binding of the clathrin-binding domain leaving the clathrin-binding domains free to interact with the scaffold and mediate continued clustering within the cage (Fig. 7a top).

Given that the particles are about 10 nm in diameter, they have a surface area of ~314 nm^2. Assuming that one full-length peptide takes up approximately 1 nm^2 on the surface, then 314 peptides would be sufficient to completely cover the particle surface. A gold salt solution of 4.0 mM would provide 4.0 mM of potential gold atoms, which would occupy a volume of 10.2 cm^3 mol^{-1} as a crystalline solid.[34] If the gold reduction goes

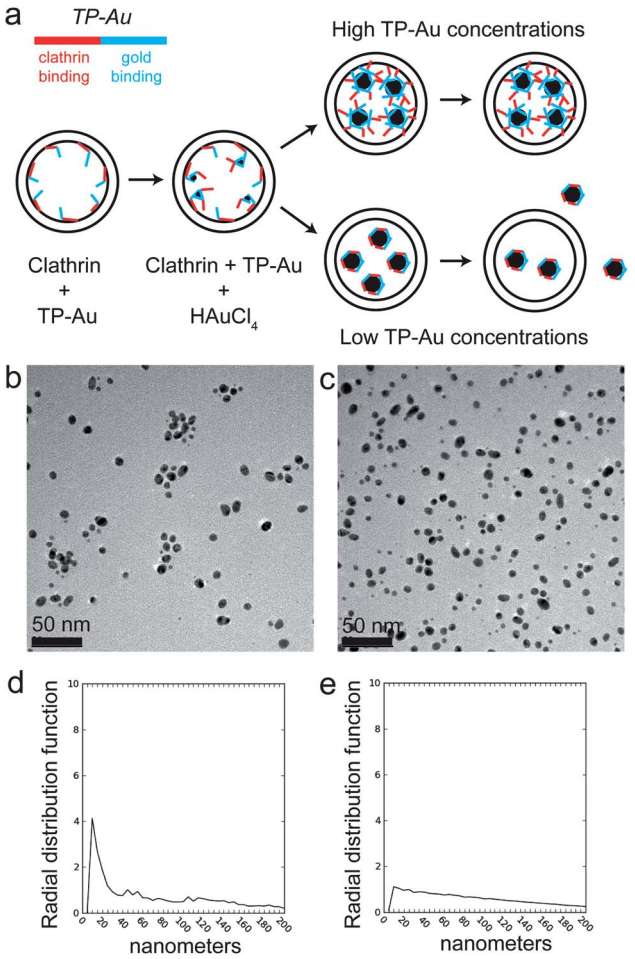

Fig. 7 (a) Schematic showing suggested particle growth mechanism in the case of high peptide concentration (top) or low peptide concentration (bottom). (b and c) TEM micrographs of gold nanoparticle synthesis reactions containing clathrin cages and 67.5 μM (b) or 33.8 μM TP-Au (c). (d and e) Radial distribution functions indicating the degree of clustering present in the TEM images of the sample containing clathrin cages and 67.5 μM (d) or 33.8 μM TP-Au (e).

to completion, then 4.0 mM of gold salt could generate 4.0×10^{19} nm^3 of gold which would be about 7.6×10^{16} particles with a diameter of 10 nm. Multiplying this value by the 314 peptides that could potentially fit on the surface of a particle, we find that 39.6 μM of peptide would cover the surface area of all of the gold particles generated if they were 10 nm in diameter. An increase in peptide concentration over this threshold value is hypothesized to lead to clathrin-binding domains becoming available as the gold-binding domains compete for space on the particle surface.

To experimentally evaluate this proposed mechanism, two synthesis reactions were carried out above and below the estimated peptide threshold concentration. These reactions previously resulted in gold nanoparticles with similar size and circularity (Fig. 3c and d). In the reaction with 67.5 μM TP-Au, the gold nanoparticles are clustered, presumably inside clathrin cages, while in the reaction with 33.8 μM TP-Au they are dispersed in solution (Fig. 7b and c). Nanoparticle clustering is also apparent in the radial distribution analysis of the images, which shows the distribution of interparticle distances (Fig. 7d and e). For particles with a diameter of 10 nm, a nearest-neighbor particle would be located 10 nm away if the two were touching. In these images the particles are not in contact so a near-neighbor peak could reasonably fall between 10 and 15 nm depending on the particle spacing. The radial distribution function has a large nearest-neighbor peak around 13 nm for the reaction with 67.5 μM TP-Au but is essentially flat for the reaction with 33.8 μM TP-Au indicating lack of significant clustering. These observations are consistent with our proposed mechanism and our calculated estimate for threshold peptide concentration. Taken together these data suggest that fine-tuning the number of available clathrin-binding domains on the nanoparticle surface by changing the TP-Au concentration in growth reactions controls the 3D arrangement of nanoparticles.

Another possible explanation for the difference in 3D arrangement of the synthesized nanoparticles is that the local concentration of TP-Au peptide inside the clathrin cage at different total peptide concentrations may be different enough to change the nature of the particle nucleation and growth within the cages. We have previously measured the dissociation constant between TEThER peptide and the clathrin foot to be about 0.24 μM.[20] Examining the two TP-Au concentrations on either side of the proposed threshold concentration required for the clustering of particles, 33.8 μM and 67.5 μM, the occupancy of clathrin feet in the reaction mixture is estimated to be 99.3% and 99.6% respectively. In a single clathrin cage, this would be a difference of 1 or 2 peptides at most, which does not seem to indicate the difference in bound peptides before nucleation and growth is the primary driver for the difference in clustering.

These data provide strong evidence that the clathrin-peptide nanoreactor forms a multi-component surfactant complex that can not only nucleate and grow nanoparticles at specific locations, *i.e.* inside the clathrin cages, but also control their 3D spatial organization after growth. In certain peptide concentration regimes, the particles remain bound to the clathrin forming 3D clusters, which are a desirable architecture for certain imaging and spectroscopy techniques.[35,36] In other concentration regimes the particles are released from the cage, in which case the cages act to direct only the initial nucleation of the particles. Further, if the clathrin nanoreactors themselves were spatially organized within a matrix or on a surface, these two separate synthesis conditions would lead to dramatically different distributions of nanomaterials in the final system.

Conclusion

We demonstrate that clathrin assemblies can be combined with engineered peptides and used as nanoreactors to generate different arrangements of gold nanoparticles. The engineered peptides fulfill multiple roles during the synthesis process which allows the clathrin nanoreactors to be fine-tuned: above a threshold peptide concentration the gold particles are made to cluster inside the clathrin nanoreactors, while below the threshold the nanoreactors are programmed to release the

particles leading to a dispersed colloidal solution. We propose a mechanism for this behavior in which the surface coverage of the peptide on the growing nanoparticles plays a key role in determining the interaction of the nanoparticle with the clathrin nanoreactor interior. We are able to accurately predict the peptide concentration at which the 3D arrangement of the nanoparticles changes. Thus we have demonstrated use of an active surfactant complex that leads to tunable control over nanoparticle growth in three dimensions by modifying concentrations of engineered components. The demonstrated ability of this bioengineered surfactant complex to generate different arrangements of nanomaterials suggests its use as a building block that may lead to the ability to form complex and dynamic materials. Such materials would be of use in a range of areas including biomedical applications, sensing, and optics. The mechanistic insights gained from this work may also inspire design of novel protein-based systems for tunable control over nanoscale synthesis and organization in three dimensions.

Experimental

Protein purification

Clathrin-coated vesicles were isolated from bovine brain tissue using differential centrifugation as previously reported.[37] Bovine brain tissue was blended in an equal volume of HKM buffer (25 mM HEPES, 125 mM potassium acetate, 5 mM magnesium acetate, 1 mM DTT, pH 7.4), homogenized, and spun at 5750 × *g* for 20 minutes. The supernatant was collected and spun at 43 000 × *g* for 40 minutes. The pellets were resuspended in HKM, mixed with an equal volume of 12.5% w/v Ficoll and 12.5% w/v sucrose in HKM, sonicated for 1 minute, and spun at 25 000 × *g* for 20 minutes. The supernatant was collected, combined with 3 volumes of HKM, and spun at 35 000 × *g* for 60 minutes. Each resulting pellet of clathrin-coated vesicles was resuspended in HKM for storage. For clathrin monomer isolation, vesicles were resuspended in dissociation buffer (1 M Tris pH 7.0, 1 mM EDTA) then spun down at 22 000 × *g* for 20 minutes before loading the supernatant onto a Sepharose CL-4B gel filtration column. Fractions were analyzed by SDS-PAGE and Western blot (clathrin heavy chain monoclonal antibody X22, Calbiochem). Final pools were analyzed by mass spectrometry (Stanford PAN Facility).

Protein cage preparation

Clathrin cages were assembled by dialyzing clathrin monomers into 4 mM Tris buffer at pH 7.0 and adding 1/10 volume of 1 M MES, pH 6.0. Samples were spun down at 16 000 × *g* for 10 min, decanted, then resuspended with 100 mM MES, pH 6.0. Paraformaldehyde (16%) was added to a final concentration of 4%, and the samples were fixed at room temperature. After spinning at 16 000 × *g* for 10 min and decanting, 100 mM potassium phosphate, pH 7.0, was added to dissociate unfixed cages. Samples were spun at 16 000 × *g* for 10 min a final time and decanted to obtain fixed clathrin cages.

Nanoparticle synthesis and analysis

Peptides TP-Au and cTP-Au were obtained from GenScript, Inc. (Piscataway, NJ) at greater than 90% purity. Fixed clathrin cages resuspended in 100 mM potassium phosphate, pH 7.0 were incubated with TP-Au or cTP-Au peptide at indicated concentrations for 15 min. $HAuCl_4$ was added to 4 mM, and the solutions were allowed to react in the dark for the indicated time periods. The reactions were stopped by drop casting the solutions onto TEM grids and then rinsing away the precursor solution. Samples were drop cast onto carbon type-B, 400 mesh, copper TEM grids (Ted Pella). TEM was performed on an FEI Tecnai G2 F20 X-TWIN operated at 200 kV. Nanoparticle size distribution and circularity were obtained using standard analysis tools in ImageJ (NIH freeware). Radial distribution functions of particle centers were calculated using lab-written code.

Acknowledgements

A. P. S. acknowledges support from a Stanford Bio-X fellowship and an Achievement Rewards for College Scientists Foundation (ARCS) Scholarship. This work is supported by the Department of Energy Office of Basic Energy Sciences, Materials Sciences and Engineering Division, under contract DE-AC02-76SF00515.

References

1 J. Turkevich, P. C. Stevenson and J. Hillier, *Discuss. Faraday Soc.*, 1951, **11**, 55–75.
2 N. G. Bastús, J. Comenge and V. Puntes, *Langmuir*, 2011, **27**, 11098–11105.
3 Y. Sun and Y. Xia, *Adv. Mater.*, 2002, **14**, 833.
4 N. R. Jana, L. Gearheart and C. J. Murphy, *J. Phys. Chem. B*, 2001, **105**, 4065–4067.
5 S.-H. Wu and D.-H. Chen, *J. Colloid Interface Sci.*, 2004, **273**, 165–169.
6 R. J. Macfarlane, B. Lee, M. R. Jones, N. Harris, G. C. Schatz and C. A. Mirkin, *Science*, 2011, **334**, 204–208.
7 D. Sun and O. Gang, *J. Am. Chem. Soc.*, 2011, **133**, 5252–5254.
8 K. Nam, D. Kim, P. Yoo, C. Chiang, N. Meethong, P. Hammond, Y. M. Chiang and A. M. Belcher, *Science*, 2006, **312**, 885–888.
9 M. Ł. Górzny, A. S. Walton and S. D. Evans, *Adv. Funct. Mater.*, 2010, **20**, 1295–1300.
10 P. Atanasova, D. Rothenstein, J. J. Schneider, R. C. Hoffmann, S. Dilfer, S. Eiben, C. Wege, H. Jeske and J. Bill, *Adv. Mater.*, 2011, **23**, 4918–4922.
11 S. S. Behrens, *J. Mater. Chem.*, 2008, **18**, 3788–3798.
12 M. Uchida, M. T. Klem, M. Allen, P. Suci, M. Flenniken, E. Gillitzer, Z. Varpness, L. O. Liepold, M. Young and T. Douglas, *Adv. Mater.*, 2007, **19**, 1025–1042.
13 J. Ge, J. Lei and R. N. Zare, *Nat. Nanotechnol.*, 2012, **7**, 428–432.
14 O. Romero, M. Filice, B. de L. Rivas, C. Carrasco-Lopez, J. Klett, A. Morreale, J. A. Hermoso, J. M. Guisan, O. Abian and J. M. Palomo, *Chem. Commun.*, 2012, **48**, 9053–9055.
15 K. K. W. Wong and S. Mann, *Adv. Mater.*, 1996, **8**, 928–932.

16 L. Zhang, J. Swift, C. A. Butts, V. Yerubandi and I. J. Dmochowski, *J. Inorg. Biochem.*, 2007, **101**, 1719–1729.
17 M. T. Klem, M. Young and T. Douglas, *J. Mater. Chem.*, 2010, **20**, 65–67.
18 H. Bai, F. Xu, L. Anjia and H. Matsui, *Soft Matter*, 2009, **5**, 966–969.
19 S. Behrens, A. Heyman, R. Maul, S. Essig, S. Steigerwald, A. Quintilla, W. Wenzel, J. Buerck, O. Dgany and O. Shoseyov, *Adv. Mater.*, 2009, **21**, 3515–3519.
20 A. P. Schoen, D. T. Schoen, K. N. L. Huggins, M. A. Arunagirinathan and S. C. Heilshorn, *J. Am. Chem. Soc.*, 2011, **133**, 18202–18207.
21 T. Kirchhausen, *Annu. Rev. Biochem.*, 2000, **69**, 699–727.
22 J. Heuser and T. Kirchhausen, *J. Ultrastruct. Res.*, 1985, **92**, 1–27.
23 M.-C. Daniel and D. Astruc, *Chem. Rev.*, 2004, **104**, 293.
24 J. L. West and N. J. Halas, *Annu. Rev. Biomed. Eng.*, 2003, **5**, 285–292.
25 S. K. Ghosh and T. Pal, *Chem. Rev.*, 2007, **107**, 4797–4862.
26 C. J. Murphy, A. M. Gole, J. W. Stone, P. N. Sisco, A. M. Alkilany, E. C. Goldsmith and S. C. Baxter, *Acc. Chem. Res.*, 2008, **41**, 1721–1730.
27 A. Fotin, Y. Cheng, P. Sliz, N. Grigorieff, S. C. Harrison, T. Kirchhausen and T. Walz, *Nature*, 2004, **432**, 573–579.
28 E. ter Haar, S. Harrison and T. Kirchhausen, *Proc. Natl. Acad. Sci. U. S. A.*, 2000, **97**, 1096–1100.
29 J. Slocik, J. Moore and D. Wright, *Nano Lett.*, 2002, **2**, 169–173.
30 R. Djalali, Y. Chen and H. Matsui, *J. Am. Chem. Soc.*, 2002, **124**, 13660–13661.
31 S. L. Westcott, S. J. Oldenburg, T. R. Lee and N. J. Halas, *Chem. Phys. Lett.*, 1999, **300**, 651–655.
32 E. Prodan, C. Radloff, N. J. Halas and P. Nordlander, *Science*, 2003, **302**, 419–422.
33 S. K. Stanley, M. L. Becker, E. K. Lin and W.-L. Wu, *Langmuir*, 2009, **25**, 10886–10892.
34 C. N. Singman, *J. Chem. Educ.*, 1984, **61**, 137.
35 A. K. Murthy, R. J. Stover, A. U. Borwankar, G. D. Nie, S. Gourisankar, T. M. Truskett, K. V. Sokolov and K. P. Johnston, *ACS Nano*, 2013, **7**, 239–251.
36 O. K. Zahr and A. S. Blum, *Nano Lett.*, 2012, **12**, 629–633.
37 A. P. Jackson, *Methods Mol. Biol.*, 1993, **19**, 83–96.

